A convergent extracellular metabolome of live contrast-enhancing human gliomas

Authors: Cecile Riviere-cazaux[1], Lucas P. Carlstrom[1], Karishma Rajani[1], Amanda Munoz-casabella[1], Masum Rahman[1], Ali Gharibi-Loron[1], Desmond Brown[2], Jaclyn J. White[3], Benjamin T. Himes[4], Ignacio Jusue-Torres[1], Samar Ikram[1], Seth Ransom[1], Renee Hirte[1], Ju-Hee Oh[5], William F. Elmquist[5], Jann N. Sarkaria[6], Rachael A. Vaubel[7], Moses Rodriguez[8], Arthur Warrington[1,8], Sani H. Kizilbash[9], Terry C. Burns[1]

Affiliations:

Departments of [1]Neurological Surgery, [6]Radiation Oncology, [7]Laboratory Medicine and Pathology, [8]Neurology, and [9]Oncology, Mayo Clinic, Rochester MN, USA

[2]Neurosurgical Oncology Unit, Surgical Neurology Branch, National Institutes of Neurological Disorders and Stroke, National Institutes of Health, Bethesda, MD, USA

[3]Department of Neurological Surgery, Wake Forest Baptist Health, Winston-Salem, NC, USA

[4]Department of Neurological Surgery, Albert Einstein College of Medicine, Montefiore Medical Center, Bronx, NY, USA

[5]Brain Barriers Research Center, Department of Pharmaceutics, College of Pharmacy, University of Minnesota, Minneapolis, MN, USA

Running title: Live human glioma extracellular metabolome

Corresponding Author Terry Burns, M.D., Ph.D.
Department of Neurosurgery – Mayo Clinic
200 First St SW
Rochester, MN, USA 55905

burns.terry@mayo.edu

Telephone: 507-284-2871 Fax: 507-284-5206

Funding: National Institute of Health: T32GM065841 to CRC, K12 NRCDP to TB, Minnesota Partnership for Biotechnology and Genomics, Mayo Clinic Cancer Center and Center for Individualized Medicine, U54 CA210180, the American Brain Tumor Association, Brains Together for the Cure, Humor to fight the Tumor, and Lucius & Terrie McKelvey.

Conflict of Interest: None.

Authorship:

- Study design and conception: TB, CRC, LPC, KR, WE
- Performed experiments: TB, CRC, LPC, KR, JW, DB
- Analyzed data: TB, CRC, KR
- Critically reviewed manuscript: all authors

Word count: 6,405

Abstract

Background: Gliomas present a formidable challenge for translational progress. Cancer metabolism is of increasing interest to understand candidate therapeutic vulnerabilities, but few methods exist to evaluate live human malignancies. We sought to characterize the global extracellular metabolome of diverse human gliomas during standard-of-care craniotomies.

Methods: We utilized high molecular weight (HMW) microdialysis with elevated flow rate pumps under an investigational device exemption to sample the microenvironments of fourteen live human gliomas and adjacent brain during fifteen neurosurgical resections. The global signature of recovered microdialysate was evaluated via ultra-performance liquid chromatography tandem mass spectrometry (UPLC-MS/MS); enrichment and correlation analyses were utilized to identify reproducible tumor phenotypes across patients in discovery and validation cohorts.

Results: 162 named metabolites were identified in at least 40 of 44 catheters from 20 μL of microdialysate representing 10 minutes of intra-operative collection time. Rank-based and correlation analyses highlighted metabolic heterogeneity across and between patients, as well as marked metabolic convergence across the contrast-enhancing regions of molecularly diverse tumors. Guanidinoacetate (GAA) demonstrated the highest differential abundance between contrast-enhancing tumor and brain adjacent to tumor.

Conclusions: A reproducible extracellular metabolic signature defines the contrast-enhancing region of molecularly diverse astrocytomas, as compared to each patient's adjacent brain.

Keywords: Glioma, microdialysis, metabolomics, isocitrate dehydrogenase

Introduction

Diffuse infiltrative gliomas, including astrocytomas and oligodendrogliomas, comprise most adult primary malignant brain tumors and remain incurable, regardless of the best available therapies[1]. Isocitrate dehydrogenase (IDH) mutations occur in all oligodendrogliomas and a subset of astrocytomas, affording improved prognosis due to typically slower growth and more favorable response to standard-of-care radiation and alkylating chemotherapy[2,3]. Highlighting the dismal rate of therapeutic progress, the last drug found to improve survival for gliomas was temozolomide in 2005[1]. Glioma heterogeneity among patients hampers therapeutic generalizations across diverse patient cohorts. Moreover, profoundly diverse genetic, epigenetic, and metabolic phenotypes accumulate within individual patients' tumor ecosystems[4,5]. Such heterogeneity has hampered therapeutic efforts to target glioma-associated mutations. Conversely, divergent gliomas may nonetheless leverage convergent metabolic survival strategies in the setting of nutrient deprivation, genotoxic stress, and growth requirements common across tumors[6,7]. As such, several features of glioma metabolism are increasingly viewed as promising therapeutic targets. Few strategies currently exist to characterize the metabolic landscape of human gliomas *in situ*.

Microdialysis has been used to quantify human extracellular biomarkers of traumatic and hypoxic brain injury in neurocritical care units. Microdialysis is also a well-established method to quantify central nervous system (CNS) drug delivery in early phase clinical trials[8-10] and has been used longitudinally to study metabolites present in human gliomas when compared to adjacent brain[11,12]. However, while some studies have utilized intraoperative microdialysis to enable quantification of select extracellular metabolites[13-15], no study thus far has deployed intra-operative microdialysis to characterize the global extracellular glioma metabolome. To that end, we initiated a pilot feasibility study leveraging high molecular weight (HMW) microdialysis

catheters in 5 surgeries, followed by validation in 10 additional surgeries to characterize the global extracellular metabolome of glioma across multiple regions of diverse gliomas. Our findings provide evidence for both divergent and convergent metabolism within and between live human brain tumors and suggest that IDH status alone is insufficient to predict the global extracellular metabolic signature of live human gliomas.

MATERIALS AND METHODS

Patient Cohort, Study Design, and Intraoperative Microdialysis

All study procedures were approved by the Mayo Clinic Institutional Review Board (IRB). Patients provided written informed consent to participate in NCT04047264--an ongoing study evaluating the safety and feasibility of intraoperative high molecular weight (100 kDa) microdialysis under an investigational device exemption. Study eligibility includes adults (>18yo) undergoing a clinically indicated surgery for known or suspected glioma. Each patient (n=14; 15 surgeries; **Fig. 1**) underwent intraoperative microdialysis using up to three M-dialysis 100 kDA catheters and 107 variable rate microdialysis pumps under an investigational device exemption across radiographically diverse regions (**Fig. 2A-B**). See supplemental methods for details of microdialysis, pathology, and molecular tumor analyses.

Targeted Analysis of D/L-2-HG

Targeted metabolomic analysis of microdialysate was performed by the Mayo Clinic metabolomic core facility. L and D isomers of 2-hydroxyglutaratic acid were derivatized and quantified by liquid chromatography mass spectrometry (LC/MS) using slight modifications to previously described methods[16-18]. See the Supplemental Methods for details.

Untargeted Metabolomic Analysis

Untargeted metabolomic analysis was performed by Metabolon, Inc. Ultra-performance liquid chromatography tandem mass spectrometry (UPLC-MS/MS), which combines physical

separation of liquid chromatography with the mass analysis capabilities of mass spectrometry. See the Supplemental Methods for details.

Ranked Metabolite lists

Ranked metabolite lists of tumor (Catheter X or Y) versus brain (Catheter Z) were generated from fifteen cases based on calculated fold changes of the peak area data (X/Z or Y/Z for the metabolite). This could not be done for patient Oligo[2] given the lack of brain-sampling catheter. In a discovery cohort, to determine an overall enhancing tumor-to-brain ranking for each metabolite, each patient's tumor-to-brain metabolites were ranked based on fold change (X/Z) and then averaged across all three patients for that metabolite. In the validation cohort, the individual tumor-to-brain rankings were compared against the discovery cohort enhancing tumor-to-brain ranking associated with each metabolite.

Enrichment Analysis

Gene Set Enrichment Analysis (GSEA) is the most widely utilized analytical method for rank-based analysis of data sets in biomedicine. GSEA is frequently performed using curated gene sets from the molecular signatures database (MSigDB), though custom feature sets can be used enabling enrichment analysis of metabolites rather than genes. Ranked metabolite lists were created as described above based on fold change to create metabolite libraries (.gmx file) against which these ranked lists (.rnk files) were compared to determine relative positive and negative enrichment (**Supplemental Data**). Additionally, results from Björkblom et al. were included as an external reference[19]. The number of feature sets evaluated is included in calculations to generate a normalized enrichment score and FDR for each.

MetaboAnalyst

Metabolomic analyses were performed using MetaboAnalyst (5.0), a publicly available web-based tool to analyze and visualize metabolomic data[20]. The normalized peak area data for the metabolites present across at least 40/44 catheters were entered into MetaboAnalyst without any further filtering. Assuming a monotonical rather than linear relation between

metabolites and samples, Spearman Correlation maps were generated in MetaboAnalyst based on features (metabolites present across all samples) and samples.

Statistical Analysis

Data are presented as normalized peak areas (median = 1 for each metabolite across batches) provided from Metabolon Inc. and are available in Supplemental File 1. MetaboAnalyst 5.0 was used for Spearman correlations. Enrichment Analysis was performed using GSEA 4.1.0 (Gene Set Enrichment Analysis), repurposed for metabolite set analysis using custom feature sets. Normality of metabolites in Figure 4 was tested via D'Agostino-Pearson test; a Wilcoxon signed rank test for non-parametric distributions was then performed on paired enhancing tumor and brain metabolites. Graphs were generated using GraphPad PRISM 9.1. FDR <0.05 was considered statistically significant for enrichment analysis.

RESULTS

Elevated D-2-Hydroxyglutarate (D-2-HG) in IDH-mutant tumor microdialysate

D-2-HG is markedly elevated in IDH-mutant gliomas and remains one of the best-characterized glioma oncometabolites[21]. We initiated our intra-operative microdialysis trial in a discovery cohort of five patients, three of whom had IDH-mutated gliomas (Oligo^{2}, Oligo^{3}1, and Astro$^{4\text{-mut}}$1) and two of whom had GBMs (GBM^{WT}1, GBM^{WT}2) (**Fig. 1**). To determine if D-2-HG levels in microdialysate quantitative reflect IDH status, we utilized 10 μL of a 40 μL microdialysate sample to quantify D-2-HG via targeted metabolomic analysis. D-2-HG was elevated in microdialysate from IDH-mutant as compared to IDH-wild-Type (WT) tumors (median: 27.29 versus 0.63 μM) (**Supplementary Fig. S1A**). Patient Astro$^{4\text{-mut}}$1 showed a >1000x difference in D-2-HG between non-enhancing tumor (FLAIR) and adjacent brain infiltrated by tumor (831.80 versus 0.68 μM). These data demonstrated the feasibility of intraoperative HMW microdialysis to quantify a dialyzable oncometabolite during standard-of-care surgery for tumor resection.

Untargeted metabolomics is increasingly leveraged to gain more comprehensive insights regarding the global metabolome. We utilized 20 μL of microdialysate from each catheter for untargeted metabolomic analysis via the Metabolon platform[22]. While low volumes of microdialysate precluded validation of all metabolites measured by untargeted metabolomics, enough volume was available to validate D-2-HG across untargeted and targeted metabolomic platforms. Untargeted analysis reported total 2-HG. In the discovery cohort, these were plotted against the combined stereoisomer (D-2-HG + L-2-HG) levels from targeted analyses yielding a robust correlation (R^2=0.9989) between the two platforms across a 2,500-fold concentration range (**Supplementary Fig. S1B)**, suggesting feasible quantitative comparisons from untargeted metabolomic data. Having established a strong correlation between untargeted and targeted metabolomic analyses, evaluation of the 2-HG peak area in the next cohort of 10 cases, including $GBM^{WT}2$'s repeat resection ($GBM^{WT}2B$) confirmed increased levels in IDH-mutant tumors when compared to IDH-WT tumors (21.41x average normalized peak area in IDH-mutant tumor compared to IDH-WT) (**Fig. 2C**). In line with other studies reporting occasional false-positive detection of 2-HG in IDH-WT tumors[23], one patient with an H3K27M-mutated infiltrative grade 4 astrocytoma demonstrated elevated 2-HG levels despite their next generation sequencing-confirming IDH-WT status. These data suggest that some IDH-WT tumors may produce elevated 2-HG levels via non-IDH-related mechanisms.

Global metabolomics reveals a dynamic glioma-versus-brain environment

To ensure comparison and reproducibility of metabolite levels across patients, we analyzed 162 named metabolites that were present in at least 90% of the catheters ($\geq$ 40/44 catheters). Intra-operatively, catheters were placed in radiographically distinct areas of the tumor (enhancing, non-enhancing ("FLAIR"), and/or infiltrated brain). Due to the diffuse nature of patient $Oligo^2$'s tumor, only non-enhancing tumor could be sampled.

Prior work by Björkblom et al.[24] reported a metabolic phenotype of glioblastoma microdialysate compared to that of adjacent brain. However, these studies were performed over several days,

whereas our samples were collected acutely during surgery. As such, we first asked if acute intraoperative sampling of the *in vivo* global metabolome via microdialysis could yield comparable results to that of prolonged catheter placements. We compared the fold changes to results from Björkblom et al, for their 24 significantly tumor- or brain-associated metabolites that were present in all of our catheters. Obvious discrepancies were only noted in 1 of 24 metabolites, 3-amino-2-piperidone **(Supplementary Fig. S2)**, demonstrating that 10 minutes of intraoperative sampling could reproduce previously identified glioma metabolic signatures from post-operative microdialysis.

Individualized signatures of enhancing tumor versus brain enriched across patients

Having demonstrated that our data appeared consistent with prior literature, we then proceeded to evaluate the full set of metabolites detected in at least 90% of catheters. For each patient, we ranked metabolites based on the fold change in peak area between enhancing (E) or non-enhancing tumor (NE), and brain adjacent to tumor (B) (**Fig. 1**). Despite substantial variation between patients in the relative magnitude of metabolite fold-changes between tumor and brain (**Supplementary Fig. S3)**, enhancing tumor- and brain-associated metabolites were consistent across patients in the discovery cohort (**Fig. 3A)**. This ranked order of metabolites was similarly observed in an independent validation cohort of patients with enhancing gliomas **(Fig. 3A)**. Top tumor-associated metabolic pathways included amino acid-associated metabolic pathways (KEGG), including leucine, isoleucine, and valine metabolism, in addition to carnitine metabolism. Brain-associated metabolic pathways included aminosugar, pentose, and alanine and aspartate metabolism.

To more rigorously and quantitatively compare metabolic phenotypes between catheters and between patients, we utilized enrichment analysis, to statistically identify similarities between and across patients' catheters. Although generally applied to gene-based analyses, we repurposed this for metabolomic analysis. Using EA, we selected the top and bottom 35 metabolites based on fold change from each comparison and determined where these

metabolites fell in the ranked metabolite lists for the remaining patients (**Supplemental Data**). In patients with enhancing astrocytomas, each patient's individual tumor signature was robustly and positively enriched in the ranked list of enhancing tumor versus brain metabolites from other patients (**Fig. 3B).** Conversely, the tumor-infiltrated brain signatures were negatively enriched in these same patient-specific tumor versus brain metabolite lists, consistent with a conserved metabolic signature of tumor versus infiltrated brain across patients (**Fig. 3C)**. Leveraging these individual patient-level data, metabolite enrichment between patients proved highly robust with a False Discovery Rate (FDR) of 0.000 for most interpatient comparisons (**Fig. 3D)** of enhancing tumor versus brain metabolites. For independent reference, the previously published metabolic signature of tumor versus adjacent brain from Björkblom et al[19] was evaluated and found to be strongly enriched at FDR of 0.002 or less for each of the enhancing astrocytomas (**Fig 3D)**. We also asked if the signature of enhancing and non-enhancing catheters is similar, utilizing enrichment analysis. Although similarities to non-enhancing catheters were observed for a subset of enhancing tumors ($GBM^{WT}1$, $GBM^{WT}4$, and H3K27M-$Astro^{4\text{-}WT}$), most comparisons between enhancing and non-enhancing catheters revealed no significant enrichment (**Supplementary Fig. S4A)**.

Metabolites of the enhancing glioma extracellular microenvironment

After demonstrating that the discovery and validation cohorts revealed a conserved metabolic signature in enhancing astrocytomas via two orthogonal methods, we then asked which metabolites defined the extracellular microenvironment across the full cohort of all 9 surgeries, two of which comprised patient $GBM^{WT}2$'s primary and recurrent tumor. Using a Wilcoxon rank sum test for non-parametric distributions, paired enhancing vs. brain catheters revealed 39 elevated metabolites in the enhancing tumor catheter and 22 elevated metabolites in the brain catheter using cutoff criteria of p-value$\leq$0.05 and FC$\geq$2 (**Fig. 4A)**. The top enhancing astrocytoma metabolite was guanidinoacetate (GAA) (FC (E/B) = 126.32x; p=0.0039), which, to our knowledge, has not previously been reported in the context of glioma (**Fig**. **4B).** The

enhancing glioma signature was also defined by greater relative abundance of proline (FC=10.1x), carnitine-family metabolites (deoxycarnitine, carnitine, and acetylcarnitine at FC= 8.71x, 7.65x, and 7.47x, respectively), and N6-methyllysine (FC=7.17x) (all at p=0.0039).

Enhancing vs. non-enhancing glioma metabolic signatures

To our knowledge, the extracellular metabolic signature of non-enhancing gliomas has not been previously reported. In 8 of 9 enhancing cases, one catheter was placed in non-enhancing (T2 hyperintense) tumor. Our cohort also included individuals with entirely non-enhancing tumors, including four oligodendrogliomas and a molecular GBM. One enhancing tumor (gemistocytic astrocytoma WHO) was very firm preventing catheter placement in the enhancing portion, thus 2 non-enhancing locations were sampled. To understand the metabolome of non-enhancing glioma, we again utilized enrichment analysis to determine if we could identify a reproducible metabolic signature across non-enhancing catheters. Non-enhancing catheters from patients with enhancing tumors tended to be enriched for each other, as well as for the signature of enhancing catheters. Conversely, catheters from entirely non-enhancing tumors were rarely enriched for each other or for the enhancing tumor signature, with exception of one catheter from Oligo^{3}1. (**Supplementary Fig. S4B)**. This could suggest either 1) conserved glioma metabolism between enhancing and non-enhancing regions of contrast-enhancing gliomas or 2) diffusion of enhancing-region metabolites into areas of non-enhancing tumors.

To determine how non-enhancing glioma metabolism compared to the enhancing portion of the tumor, we utilized non-enhancing vs. enhancing ranked lists from our 8 patients with paired enhancing and non-enhancing catheters. Enrichment analyses revealed that the non-enhancing vs. enhancing portion of the glioma was significantly enriched for the brain metabolome across patients (FDR<0.004 for most patients) (**Supplementary Fig. S4C)**. This suggests that non-enhancing portion of enhancing tumors has a metabolic signature that is intermediate between enhancing tumor and brain. In summary, intraoperative microdialysis

revealed a conserved global tumor versus brain signature in extracellular fluid, particularly for enhancing astrocytomas. Importantly, rank-based analyses empowered statistical comparisons of individual patients' glioma metabolomes to each other.

Metabolite and patient correlation analyses

Individualized intra-patient catheter comparisons were utilized for most analyses of our intraoperative microdialysis samples. Having now identified a conserved metabolic signature across enhancing astrocytomas, with some enrichment in the non-enhancing catheters of those tumors, we asked how patients' catheters would correlate and cluster across all samples. As expected based on our robust metabolic signature, Spearman correlation of all 44 catheters revealed clustering of the enhancing grade 4 astrocytoma catheters (**Fig. 5A**). Interestingly, catheters from patients with oligodendrogliomas clustered based on the patient's identity. Clustering of non-enhancing astrocytoma catheters was variable, but those clustering with the enhancing catheters (Astro$^{4\text{-mut}}$1, Astro$^{4\text{-mut}}$2, Astro$^{4\text{-mut}}$3, and GemAstro$^{3\text{-mut}}$) tended to have enrichment for enhancing catheters in GSEA (**Supplementary Fig. S4B)**. We separately performed Spearman correlation considering only the catheters of patients with enhancing grade 4 astrocytomas. Results again confirmed clustering of most enhancing catheters, except for GBM^{WT}1 which clustered with non-enhancing catheters. Interestingly, the tumor of our one patient for whom microdialysis was performed twice (primary and recurrent: GBM^{WT}2 and 2B, respectively) clustered next to each other in both analyses. In general, most non-enhancing catheters tended to cluster together, although some did cluster with the brain catheters (H3K27M-Astro$^{4\text{-WT}}$ **Fig. 5B)**. Surprisingly, no obvious clustering by IDH status or recurrence status was observed. Spearman correlation of the 162 metabolites again suggested covariance of enhancing catheter-associated amino acid and carnitine metabolism. Brain catheter-associated metabolites also clustered together (**Supplementary Fig. S5).** In sum, results of correlation analyses suggest that the extracellular metabolome of molecularly diverse enhancing astrocytoma catheters clustered by region, whereas that of oligodendroglioma

catheters clustered by patient. Furthermore, non-enhancing glioma metabolism may exist on a spectrum between enhancing tumor and brain metabolism based on the variable clustering of these catheters with enhancing or brain-sampling catheters.

DISCUSSION

We tested the feasibility of intraoperative microdialysis to acutely evaluate the extracellular metabolome within live human gliomas immediately prior to resection. This rarely leveraged window of opportunity within a standard-of-care glioma resection demonstrated: 1) robustly elevated D-2-HG in IDH-mutant glioma microdialysate; 2) metabolic features that reproducibly separate enhancing tumor from brain across molecularly and clinically diverse astrocytomas; and 3) lack of clustering by IDH-status or recurrence status.

Acute intraoperative microdialysis in a practical timeframe yielded relative levels of hundreds of metabolites for targeted and untargeted metabolomics analyses in fourteen patients with molecularly clinically diverse gliomas, including one patient's primary and recurrent tumor. Increasing preclinical evidence suggests the potential therapeutic utility of targeting cancer-associated metabolic vulnerabilities. In contrast to the profound genomic heterogeneity seen within and across malignancies, a more finite set of convergent metabolic strategies might be deployed to meet the unavoidable bioenergetic demands of tumor metabolism[25] in the face of genomic instability[26,27], oxidative stress[28], hypoxia[29], and nutrient deprivation[30,31]. Microdialysis surprisingly revealed a highly conserved and reproducible tumor metabolic signature of enhancing grade 4 astrocytomas whose samples differed across multiple clinical and technical parameters (**Fig. 1; Supplemental Table 1**). Moreover, our rank-based analyses confirmed a set of glioma versus brain-associated metabolites identified in a previously published study of post-operative microdialysis (**Supplementary Fig. S2; Fig 3D**;[19]). Technical methodology in the post-operative study varied significantly from ours and was performed by an independent team on a different continent confirming the robust nature of the enhancing glioma metabolome.

Such interpatient and interstudy reproducibility in the enhancing tumor-versus-brain extracellular metabolome could suggest therapeutically targetable metabolic convergence across primary and recurrent IDH-mutant and IDH-wildtype astrocytomas.

IDH-mutant gliomas epitomize the oncogenic relevance of altered metabolism. We found elevated D-2-HG in the microdialysate in IDH-mutant tumors (**Supplementary Fig. 1; Fig. 2C**). D-2-HG was previously used as a pharmacodynamic biomarker for IDH inhibitors in tissue[32] and via magnetic resonance spectroscopy[33-35]. Our observations suggest that monitoring of extracellular D-2-HG via microdialysis could provide an additional tool to augment early phase translation of novel therapies. Interestingly, D-2-HG was higher in the non-enhancing than enhancing tumor in 3/3 patients with catheters in both regions of enhancing IDH-mutant tumors, suggesting that some tumor metabolites may either be lost down a disrupted blood brain barrier or may be produced at lower levels in relatively more hypoxic tumor regions.

Importantly, although IDH-mutations are thought to drive early tumorigenic metabolic and epigenetic changes, the global extracellular metabolome of enhancing astrocytoma was highly reproducible across all analyses despite differences in IDH status. Interestingly, oligodendrogliomas clustered based on patient identity and were rarely enriched for other oligodendrogliomas' or astrocytomas' metabolomes (**Fig. 5; Supplementary Fig. S4B)**. Recently published work from over 200 glioma tissues demonstrated significant metabolic heterogeneity in IDH-mutant gliomas and separation of IDH-mutant from IDH-WT tumors, albeit with fewer metabolites differentiating IDH-mutant grade 4 astrocytomas from GBMs[36]. Lack of a metabolic signature of IDH-mutant gliomas beyond elevated 2-HG in our data could be due to a smaller cohort of patients lacking in low-grade astrocytomas. Indeed the clustering of grade 4 IDH-mutant astrocytomas with lower grade IDH-mutant gliomas in tissue metabolomic analyses was solely dependent on 2-HG[36]. Future studies will be needed to directly compare the extracellular versus tissue metabolome in paired patient samples. Taken together, our

extracellular metabolic data suggest that despite markedly elevated D-2-HG production, IDH-mutant grade 4 astrocytomas may evolve into lesions which are otherwise almost metabolically indistinguishable from IDH-WT grade 4 astrocytomas. Having demonstrated the safety and feasibility of intraoperative microdialysis, recent expansion of our ongoing study will enable us to identify metabolic convergencies and divergencies across a larger and more diverse cohort of patients, including lower-grade astrocytomas. Further work will define the extent to which patient gender and tumor grade, in addition to clinical variables, may contribute to extracellular metabolic phenotype.

To our knowledge, our data report on a larger number of extracellular metabolites and patients than any prior study evaluating the live human glioma extracellular metabolome. Although small volumes of intraoperatively collected microdialysate enabled discovery of a large number of differentially abundant analytes via UPLC-MS/MS, analytes of potential therapeutic interest will require further validation via targeted analyses. Many of the enhancing tumor-associated metabolites confirm metabolic disruptions such as upregulation of amino acids, including proline[37], asparagine[38], and amino acid derivatives, such as N6-methyllysine, which have been reproducibly associated with cancer biology[39]. Accumulation of these metabolites may suggest an adaptive response to nutrient deprivation observed in gliomas[38,40,41] and other cancers[42]. Multiple carnitine family metabolites were among the top tumor-associated metabolites (**Fig. 4**) and have been linked to energy production via fatty acid oxidation in glioma[43,44].

The top tumor-associated metabolite in our data was guanidinoacetate (GAA) (**Fig. 4)**, which accumulates in patients with GAMT deficiency, leading to impaired creatine production, seizures, and cognitive impairment[45]. To our knowledge, GAA elevation has not previously been reported in glioma, perhaps reflecting infrequent analysis of extracellular metabolites. While creatine levels were not elevated in tumor, GAA is also co-produced with ornithine, the precursor to polyamine synthesis. Polyamine synthesis via ornithine decarboxylase (ODC) is

upregulated in cancers, including glioblastoma, to support catabolic demand, regulate intracellular pH in the acidic tumor core, and protect against immune surveillance[46]. It is therefore tempting to speculate that increased GAA could be indicative of increased polyamine synthesis within gliomas. If confirmed, longitudinal monitoring of GAA may augment translational studies targeting glioma polyamine synthesis. Indeed, combined blockade of ODC and polyamine transporters via DFMO and AMXT-1501, respectively, prolonged survival in preclinical models of multiple cancers, including diffuse midline gliomas[47,48]. We recently secured an investigational new drug (IND) approval for dual polyamine inhibition, during which we will utilize post-operative microdialysis to evaluate GAA as a pharmacodynamic biomarker of polyamine synthesis, *in situ*.

One limitation of microdialysis is that it does not discriminate analytes generated by the tumor from those entering the tumor microenvironment through a disrupted blood-brain barrier. One recent intraoperative study compared metabolites within the glioma's arterial versus venous supply to determine which were consumed versus produced by the gliomas[49]. However, paired analysis of adjacent brain was not performed to discriminate tumor- from brain-associated metabolism. The combination of intra-operative microdialysis and tumor vascular sampling would help elucidate the origin of enhancing tumor-associated metabolites. Additionally, future studies could utilize focally delivered isotopes via reverse microdialysis to evaluate glioma metabolic consumption and production, *in situ*.

In summary, we have shown that intraoperative microdialysis for analysis of the global extracellular tumor metabolome is feasible and empowers previously unleveraged access to each patient's diverse tumor. Our patients understand the formidable odds of their disease. We present their data as a first installment toward what we intend to be a growing collaborative, open-source repository of individualized data from live human gliomas. We (both patients and investigators) hope that the data and insights shared can help inspire novel translational

paradigms. By leveraging neurosurgical access to live human disease, we hope to accelerate tangible progress within the lifetimes of individual patients.

Funding: CRC was supported by National Institute of Health, T32GM065841; TCB was supported by NIH K12 NRCDP, R61NS122096, Minnesota Partnership for Biotechnology and Genomics, Mayo Clinic Cancer Center and Center for Individualized Medicine, the American Brain Tumor Association, Brains Together for the Cure, Humor to fight the Tumor, and Lucius & Terrie McKelvey; support was also provided by U54 CA210180 and U19 CA264362-01(JNS).

Acknowledgements: We would like to thank each of our patients who selflessly participated in this study and without whom this work and any advancement in the field of neuro-oncology would not be possible. We also thank Elizabeth Oishi for regulatory support and the Mayo Clinic Neurosurgery Clinical Research team, and the Mayo neurosurgery operative staff for their invaluable support.

References

1. Stupp R, Mason WP, van den Bent MJ, et al. Radiotherapy plus concomitant and adjuvant temozolomide for glioblastoma. *The New England journal of medicine.* 2005; 352(10):987-996.

2. Yan H, Parsons DW, Jin G, et al. IDH1 and IDH2 mutations in gliomas. *The New England journal of medicine.* 2009; 360(8):765-773.

3. SongTao Q, Lei Y, Si G, et al. IDH mutations predict longer survival and response to temozolomide in secondary glioblastoma. *Cancer Sci.* 2012; 103(2):269-273.

4. Shibao S, Minami N, Koike N, et al. Metabolic heterogeneity and plasticity of glioma stem cells in a mouse glioblastoma model. *Neuro Oncol.* 2018; 20(3):343-354.

5. Kondo Y, Katsushima K, Ohka F, Natsume A, Shinjo K. Epigenetic dysregulation in glioma. *Cancer Sci.* 2014; 105(4):363-369.

6. Vlashi E, Lagadec C, Vergnes L, et al. Metabolic state of glioma stem cells and nontumorigenic cells. *Proc Natl Acad Sci U S A.* 2011; 108(38):16062-16067.

7. Strickland M, Stoll EA. Metabolic Reprogramming in Glioma. *Front Cell Dev Biol.* 2017; 5:43.

8. Lynes J, Jackson S, Sanchez V, et al. Cytokine Microdialysis for Real-Time Immune Monitoring in Glioblastoma Patients Undergoing Checkpoint Blockade. *Neurosurgery.* 2019; 84(4):945-953.

9. Portnow J, Badie B, Liu X, et al. A pilot microdialysis study in brain tumor patients to assess changes in intracerebral cytokine levels after craniotomy and in response to treatment with a targeted anti-cancer agent. *J Neurooncol.* 2014; 118(1):169-177.

10. Blakeley JO, Olson J, Grossman SA, He X, Weingart J, Supko JG. Effect of blood brain barrier permeability in recurrent high grade gliomas on the intratumoral

pharmacokinetics of methotrexate: a microdialysis study. *J Neurooncol.* 2009; 91(1):51-58.

11. Marcus HJ, Carpenter KLH, Price SJ, Hutchinson PJ. In vivo assessment of high-grade glioma biochemistry using microdialysis: a study of energy-related molecules, growth factors and cytokines. *Journal of Neuro-Oncology.* 2010; 97(1):11-23.

12. Roslin M, Henriksson R, Bergstrom P, Ungerstedt U, Bergenheim AT. Baseline levels of glucose metabolites, glutamate and glycerol in malignant glioma assessed by stereotactic microdialysis. *J Neurooncol.* 2003; 61(2):151-160.

13. Melani A, De Micheli E, Pinna G, Alfieri A, Della Corte L, Pedata F. Adenosine extracellular levels in human brain gliomas: an intraoperative microdialysis study. *Neuroscience letters.* 2003; 346(1-2):93-96.

14. Bianchi L, De Micheli E, Bricolo A, et al. Extracellular levels of amino acids and choline in human high grade gliomas: an intraoperative microdialysis study. *Neurochemical research.* 2004; 29(1):325-334.

15. Homapour B, Bowen JE, Want EJ, et al. Intra-operative, real-time, three-dimensional ultrasound assisted positioning of catheters in the microdialysis of glial tumours. *Journal of Clinical Neuroscience.* 2010; 17(4):506-510.

16. Oldham WM, Loscalzo J. Quantification of 2-Hydroxyglutarate Enantiomers by Liquid Chromatography-mass Spectrometry. *Bio Protoc.* 2016; 6(16).

17. Struys EA, Jansen EE, Verhoeven NM, Jakobs C. Measurement of urinary D- and L-2-hydroxyglutarate enantiomers by stable-isotope-dilution liquid chromatography-tandem mass spectrometry after derivatization with diacetyl-L-tartaric anhydride. *Clin Chem.* 2004; 50(8):1391-1395.

18. Cheng QY, Xiong J, Huang W, et al. Sensitive Determination of Onco-metabolites of D- and L-2-hydroxyglutarate Enantiomers by Chiral Derivatization Combined with Liquid Chromatography/Mass Spectrometry Analysis. *Sci Rep.* 2015; 5:15217.

19. Bjorkblom B, Jonsson P, Tabatabaei P, et al. Metabolic response patterns in brain microdialysis fluids and serum during interstitial cisplatin treatment of high-grade glioma. *Br J Cancer.* 2020; 122(2):221-232.

20. Pang Z, Chong J, Zhou G, et al. MetaboAnalyst 5.0: narrowing the gap between raw spectra and functional insights. *Nucleic Acids Res.* 2021; 49(W1):W388-w396.

21. Waitkus MS, Diplas BH, Yan H. Isocitrate dehydrogenase mutations in gliomas. *Neuro-Oncology.* 2015; 18(1):16-26.

22. Ryals J, Lawton K, Stevens D, Milburn M. Metabolon, Inc. 2007.

23. Andronesi OC, Rapalino O, Gerstner E, et al. Detection of oncogenic IDH1 mutations using magnetic resonance spectroscopy of 2-hydroxyglutarate. *J Clin Invest.* 2013; 123(9):3659-3663.

24. Wibom C, Surowiec I, Moren L, et al. Metabolomic patterns in glioblastoma and changes during radiotherapy: a clinical microdialysis study. *J Proteome Res.* 2010; 9(6):2909-2919.

25. Bi J, Chowdhry S, Wu S, Zhang W, Masui K, Mischel PS. Altered cellular metabolism in gliomas — an emerging landscape of actionable co-dependency targets. *Nature Reviews Cancer.* 2020; 20(1):57-70.

26. Zhang Y, Li J, Yi K, et al. Elevated signature of a gene module coexpressed with CDC20 marks genomic instability in glioma. *Proceedings of the National Academy of Sciences.* 2019; 116(14):6975-6984.

27. Milinkovic V, Bankovic J, Rakic M, et al. Genomic instability and p53 alterations in patients with malignant glioma. *Exp Mol Pathol.* 2012; 93(2):200-206.

28. Huang H, Zhang S, Li Y, et al. Suppression of mitochondrial ROS by prohibitin drives glioblastoma progression and therapeutic resistance. *Nature Communications.* 2021; 12(1):3720.

29. Steinbach JP, Wolburg H, Klumpp A, Probst H, Weller M. Hypoxia-induced cell death in human malignant glioma cells: energy deprivation promotes decoupling of mitochondrial cytochrome c release from caspase processing and necrotic cell death. *Cell Death & Differentiation.* 2003; 10(7):823-832.

30. Tanaka K, Sasayama T, Nagashima H, et al. Glioma cells require one-carbon metabolism to survive glutamine starvation. *Acta Neuropathologica Communications.* 2021; 9(1):16.

31. Mondal S, Bhattacharya K, Mandal C. Nutritional stress reprograms dedifferention in glioblastoma multiforme driven by PTEN/Wnt/Hedgehog axis: a stochastic model of cancer stem cells. *Cell Death Discovery.* 2018; 4(1):110.

32. Konteatis Z, Artin E, Nicolay B, et al. Vorasidenib (AG-881): A First-in-Class, Brain-Penetrant Dual Inhibitor of Mutant IDH1 and 2 for Treatment of Glioma. *ACS Med Chem Lett.* 2020; 11(2):101-107.

33. Molloy AR, Najac C, Viswanath P, et al. MR-detectable metabolic biomarkers of response to mutant IDH inhibition in low-grade glioma. *Theranostics.* 2020; 10(19):8757-8770.

34. Andronesi OC, Arrillaga-Romany IC, Ly KI, et al. Pharmacodynamics of mutant-IDH1 inhibitors in glioma patients probed by in vivo 3D MRS imaging of 2-hydroxyglutarate. *Nat Commun.* 2018; 9(1):1474.

35. Wenger KJ, Richter C, Burger MC, et al. Non-Invasive Measurement of Drug and 2-HG Signals Using (19)F and (1)H MR Spectroscopy in Brain Tumors Treated with the Mutant IDH1 Inhibitor BAY1436032. *Cancers (Basel).* 2020; 12(11).

36. Björkblom B, Wibom C, Eriksson M, et al. Distinct metabolic hallmarks of WHO classified adult glioma subtypes. *Neuro-Oncology.* 2022; 24(9):1454-1468.

37. Burke L, Guterman I, Palacios Gallego R, et al. The Janus-like role of proline metabolism in cancer. *Cell Death Discovery.* 2020; 6(1):104.

38. Panosyan EH, Wang Y, Xia P, et al. Asparagine depletion potentiates the cytotoxic effect of chemotherapy against brain tumors. *Mol Cancer Res.* 2014; 12(5):694-702.

39. Lieu EL, Nguyen T, Rhyne S, Kim J. Amino acids in cancer. *Experimental & Molecular Medicine.* 2020; 52(1):15-30.

40. Yamashita D, Bernstock JD, Elsayed G, et al. Targeting glioma-initiating cells via the tyrosine metabolic pathway. *J Neurosurg.* 2020; 134(3):721-732.

41. Friedrich M, Sankowski R, Bunse L, et al. Tryptophan metabolism drives dynamic immunosuppressive myeloid states in IDH-mutant gliomas. *Nature Cancer.* 2021; 2(7):723-740.

42. Vettore L, Westbrook RL, Tennant DA. New aspects of amino acid metabolism in cancer. *British Journal of Cancer.* 2020; 122(2):150-156.

43. Fink MA, Paland H, Herzog S, et al. L-Carnitine-Mediated Tumor Cell Protection and Poor Patient Survival Associated with OCTN2 Overexpression in Glioblastoma Multiforme. *Clin Cancer Res.* 2019; 25(9):2874-2886.

44. Juraszek B, Czarnecka-Herok J, Nałęcz KA. Glioma cells survival depends both on fatty acid oxidation and on functional carnitine transport by SLC22A5. *Journal of Neurochemistry.* 2021; 156(5):642-657.

45. Gordon N. Guanidinoacetate methyltransferase deficiency (GAMT). *Brain Dev.* 2010; 32(2):79-81.

46. Miska J, Rashidi A, Lee-Chang C, et al. Polyamines drive myeloid cell survival by buffering intracellular pH to promote immunosuppression in glioblastoma. *Sci Adv.* 2021; 7(8).

47. Levin VA, Ictech SE, Hess KR. Clinical importance of eflornithine (alpha-difluoromethylornithine) for the treatment of malignant gliomas. *CNS Oncol.* 2018; 7(2):CNS16.

48. Khan A, Gamble LD, Upton DH, et al. Dual targeting of polyamine synthesis and uptake in diffuse intrinsic pontine gliomas. *Nat Commun.* 2021; 12(1):971.
49. Xiong N, Gao X, Zhao H, et al. Using arterial-venous analysis to characterize cancer metabolic consumption in patients. *Nat Commun.* 2020; 11(1):3169.

Figure 1. Intraoperative microdialysis patient characteristics.

The patient IDs and final pathologic diagnoses, including IDH- status and other available key molecular features, are summarized together with the catheter locations. Additional specifics regarding each patient, tumor, and catheter are available in Supplemental Table 1. *Diagnosis of IDH-WT GBM was reached for patient GBM^{WT}2/2B without need for further molecular studies.

Figure 2. Intraoperative microdialysis set-up and D-2-hydroxyglutarate (D-2-HG) detection.

(A) A representative intraoperative photograph ($Oligo^2$) demonstrating the experimental setup, including placement of three 100 kDA microdialysis catheters, as well as pumps and collection vials within the surgical field.

(B) Illustrative intraoperative trajectory views captured from the Neuronavigation system demonstrate the planned trajectory (blue line) toward the intended target location for each 10 mm microdialysis membrane (yellow box) in enhancing (Catheter X) and non-enhancing tumor (Catheter Y), in addition to relatively normal brain adjacent to tumor (Catheter Y).

(**C)** 2-hydroxyglutarate peak areas from UPLC-MS/MS were measured in the microdialysate from each of the 44 catheters. IDH status is indicated as mutant (blue) or wild type (red). Symbol shape indicates catheter placement location (see legend).

Figure 3. Conserved metabolic signature of enhancing grade 4 astrocytomas.

(**A**) 162 metabolites present in at least 40/44 catheters were ranked according to the enhancing tumor-versus-brain fold change in each patient. The rank order of each metabolite in each 2-catheter tumor/brain comparison (e.g., catheter X versus Z) is conveyed as a heat map from 1 (orange, tumor) to 162 (green, brain). Metabolites are listed based on the average of ranks of enhancing vs. brain in the discovery cohort ($Astro^{4\text{-}mut}1$, $GBM^{WT}1$ and $GBM^{WT}2$). The top 10 tumor- and brain-associated metabolites are specified. The proportion of metabolic pathways as annotated by Metabolon present in the top 20 tumor and brain metabolites are depicted by pie graphs (orange: tumor-associated, green: brain-associated, blue: not specific to either).

(**B**) Metabolites were ranked by fold change between catheter X versus Z (tumor versus brain) in each patient. The top 35 tumor- and brain-associated metabolites for each patient were used for enrichment analysis. A representative example enrichment analysis plot is shown demonstrating positive enrichment for the top 35 metabolites in $Astro^{4\text{-}mut}3$ tumor in the ranked metabolite list of $GBM^{WT}1$ tumor versus brain.

(**C**) A representative example enrichment analysis plot demonstrates negative enrichment for the top 35 brain-associated metabolites in $Astro^{4\text{-}mut}2$ brain in the ranked metabolite list of $GBM^{WT}4$ tumor versus brain.

(**D**) Normalized enrichment scores (NES) and the associated false discovery rates (FDR) are shown based upon enrichment for the top 35 tumor (enhancing, E and non-enhancing, NE)- and brain (B)-associated metabolites in the ranked metabolite of enhancing tumor vs. brain (Cath. X/Z). Enrichment for tumor metabolites identified in Björkblom et al., 2020 was also calculated to assess performance of the metabolite set enrichment strategy using an independent external tumor versus brain metabolite set.

2-O-MA: 2-O-methylascorbic acid; 2PY: N1-methyl-2-pyridone-5-carboxamide; 3M-5-aminovalerate: N,N,N-trimethyl-5-aminovalerate; DMTPA: 2,3-dihydroxy-5-methylthio-4-pentenoic acid; NAAG: N-acetylaspartylglutamic acid.

Figure 4. Enhancing tumor and brain microdialysates have distinct metabolites.

(**A)** A Wilcoxon signed-rank test and fold-changes between enhancing tumor vs. brain were utilized to construct a volcano plot (cut-offs for significance: p-value<0.05; FC$\geq$2). The top 10 enhancing tumor and brain metabolites are specified based on average fold-change across the 9 paired patient samples (all at p=0.0039). The normalized peak areas for the top six most differentially abundant metabolites in enhancing tumor vs. brain are shown in (**B)** for the 9 cases (p=0.0039 for all); colors correlate with patient identity from Figure 1.

2-O-MA= 2-O-methylascorbic acid; DMTPA = 2,3-dihydroxy-5-methylthio-4-pentenoic acid; GAA = guanidinoacetate; NAA = n-acetylaspartate; NANA = n-acetylneuraminate.

Figure 5. Microdialysate samples correlate based on patient identity and catheter location.

Spearman correlation map of the 44 catheters from all 15 microdialysis cases (14 patients) **(A)** and only enhancing grade 4 astrocytomas (**B)** using the 162 metabolites present in >90% of catheters. (Minimal correlation: -0.7, maximal correlation: 1).

Figure 1. Intraoperative microdialysis patient characteristics.

Patient ID	Pathology	IDH Status	Other molecular/genetic features	Catheter X	Catheter Y	Catheter Z
Oligo^{2}	**Oligodendroglioma** WHO 2	**Mutant**	1p/19q co-deletion; TERT-mutant	Non-enhancing (NE)	Non-enhancing (NE)	Non-enhancing (NE)
Oligo^{3}1	**Oligodendroglioma** WHO 3	**Mutant**	1p/19q co-deletion; TERT-mutant	Non-enhancing (NE)	Non-enhancing (NE)	Brain adjacent to tumor (B)
Oligo^{3}2	**Oligodendroglioma** WHO 3	**Mutant**	1p/19q co-deletion; TERT-mutant	Non-enhancing (NE)	Non-enhancing (NE)	Brain adjacent to tumor (B)
Oligo^{3}3	**Oligodendroglioma** WHO 3	**Mutant**	1p/19q co-deletion; TERT-mutant	Non-enhancing (NE)	Non-enhancing (NE)	Brain adjacent to tumor (B)
GemAstro$^{3\text{-}mut}$	**Gemistocytic Astrocytoma** WHO 3	**Mutant**	None remarkable	Non-enhancing (NE)	Non-enhancing (NE)	Brain adjacent to tumor (B)
Astro$^{4\text{-}mut}$1	**Astrocytoma** WHO 4 (Recurrent)	**Mutant**	MGMT non-methylated; loss of CDKN2A/B; complex karyotype	Enhancing (E)	Non-enhancing (NE)	Brain adjacent to tumor (B)
Astro$^{4\text{-}mut}$2	**Astrocytoma** WHO 4	**Mutant**	MGMT non-methylated; loss of CDKN2A/B	Enhancing (E)	Non-enhancing (NE)	Brain adjacent to tumor (B)
Astro$^{4\text{-}mut}$3	**Astrocytoma** WHO 4 (Recurrent)	**Mutant**	Indeterminate MGMT methylation	Enhancing (E)	Non-enhancing (NE)	Brain adjacent to tumor (B)
H3K27M-Astro$^{4\text{-}WT}$	**Infiltrating Astrocytoma** WHO 4	**Wild-type**	H3K27M, TERT-mutant; MGMT non-methylated	Enhancing (E)	Non-enhancing (NE)	Brain adjacent to tumor (B)
GBM^{WT}1	**Glioblastoma**	**Wild-type**	MGMT non-methylated; loss of CDKN2A/B; TERT-mutant	Enhancing (E)	Non-enhancing (NE)	Brain adjacent to tumor (B)
GBM^{WT}2	**Glioblastoma** (Primary)	**Wild-type**	Indeterminate MGMT methylation*	Enhancing (E)	Non-enhancing (NE)	Brain adjacent to tumor (B)
GBM^{WT}2B	**Glioblastoma** (Recurrent)	**Wild-type**	Indeterminate MGMT methylation*	Enhancing (E)		Brain adjacent to tumor (B)
GBM^{WT}3	**Glioblastoma**	**Wild-type**	MGMT non-methylated	Enhancing (E)	Non-enhancing (NE)	Brain adjacent to tumor (B)
GBM^{WT}4	**Glioblastoma** (Recurrent)	**Wild-type**	MGMT non-methylated; EGFR amplification; loss of CDKN2A/B	Enhancing (E)	Non-enhancing (NE)	Brain adjacent to tumor (B)
MolecGBM^{WT}	**Molecular Glioblastoma**	**Wild-type**	Gain of ch. 7, loss of ch. 10; TERT-mutant; MGMT non-methylated	Non-enhancing (NE)	Non-enhancing (NE)	Brain adjacent to tumor (B)

Figure 2. Intraoperative microdialysis set-up and D-2-hydroxyglutarate (D-2-HG) detection.

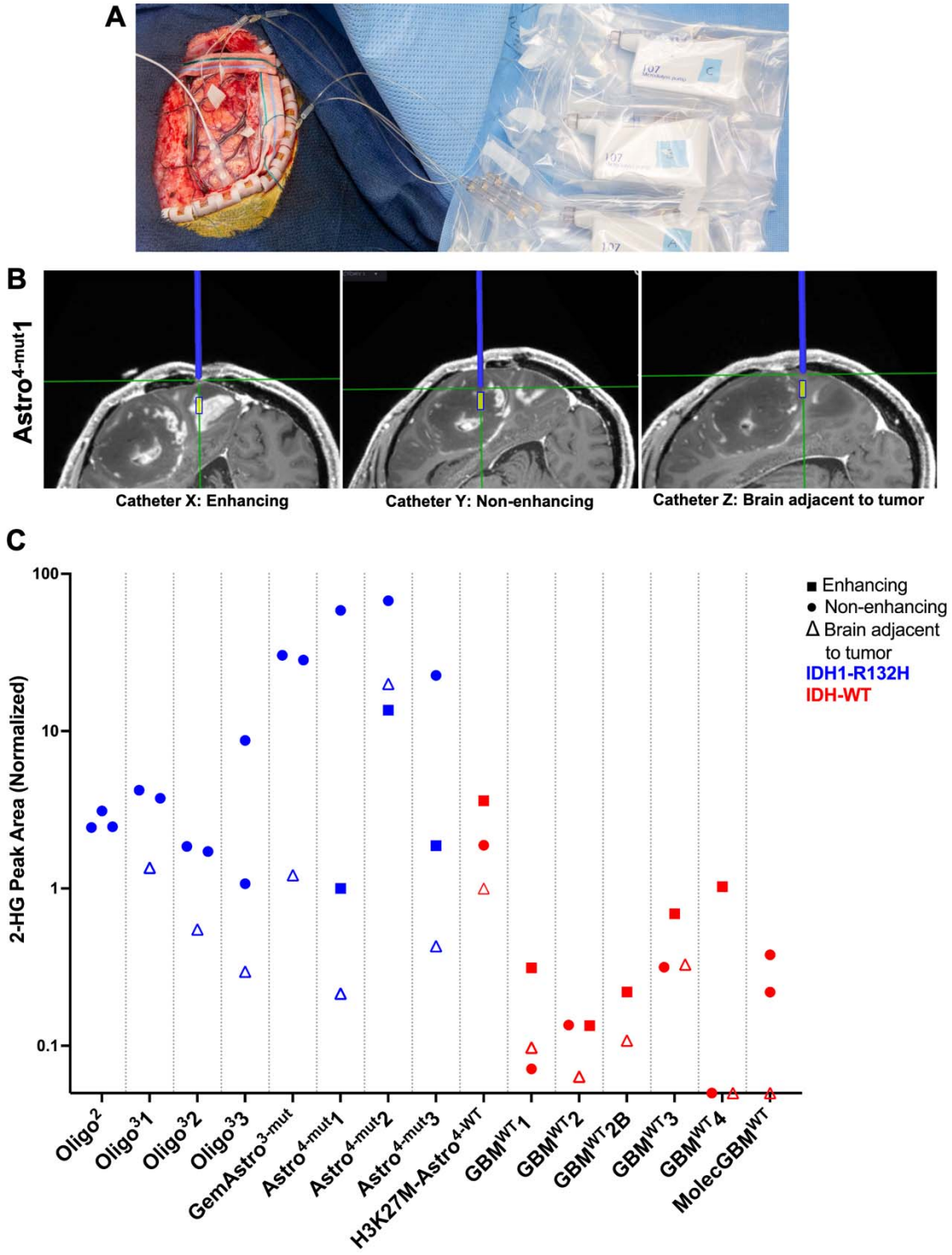

Figure 3. Conserved metabolic signature of enhancing grade 4 astrocytomas.

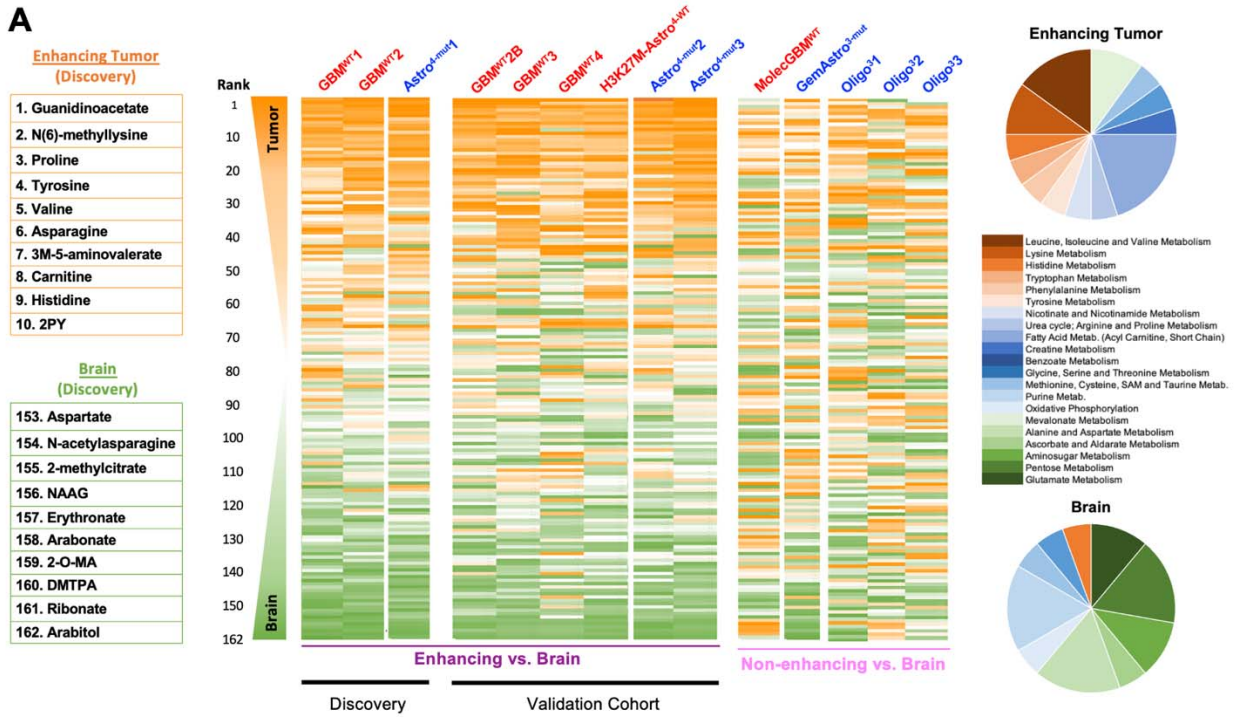

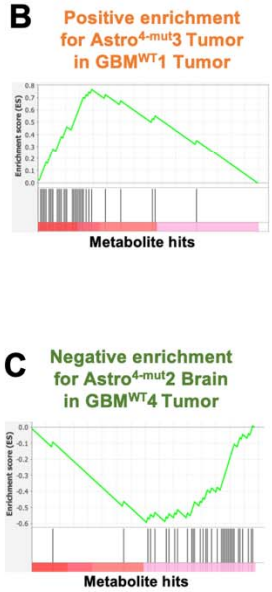

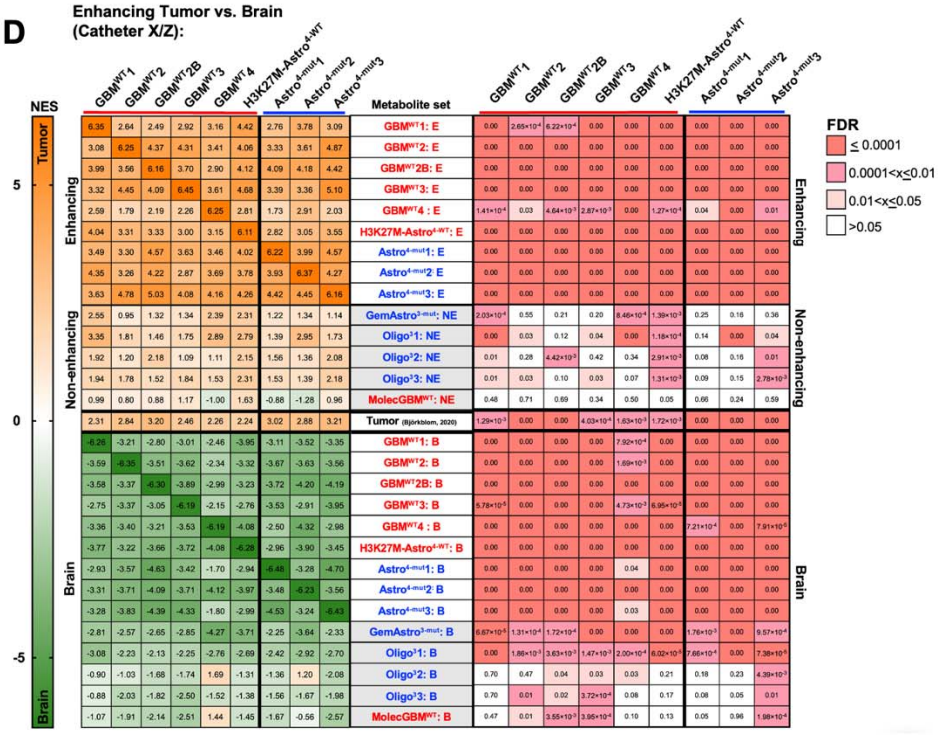

Figure 4. Enhancing tumor and brain microdialysates have distinct metabolites.

A

Brain

Metabolite	FC E/B
Arabitol	0.04
Arabonate	0.08
Ribonate	0.11
2-O-MA	0.14
DMTPA	0.15
NAA	0.17
Erythronate	0.17
N-acetylserine	0.21
Fructose	0.25
NANA	0.25

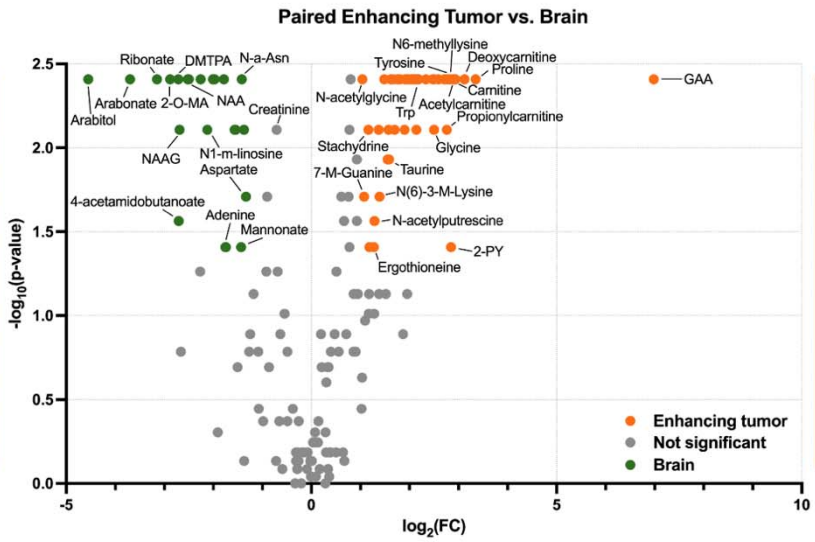

Enhancing Tumor

Metabolite	FC E/B
GAA	126.32
Proline	10.18
Deoxycarnitine	8.71
Carnitine	7.65
Acetylcarnitine	7.47
N6-methyllysine	7.17
Methionine	7.09
Dimethylglycine	6.90
Asparagine	6.84
Alanine	6.54

B

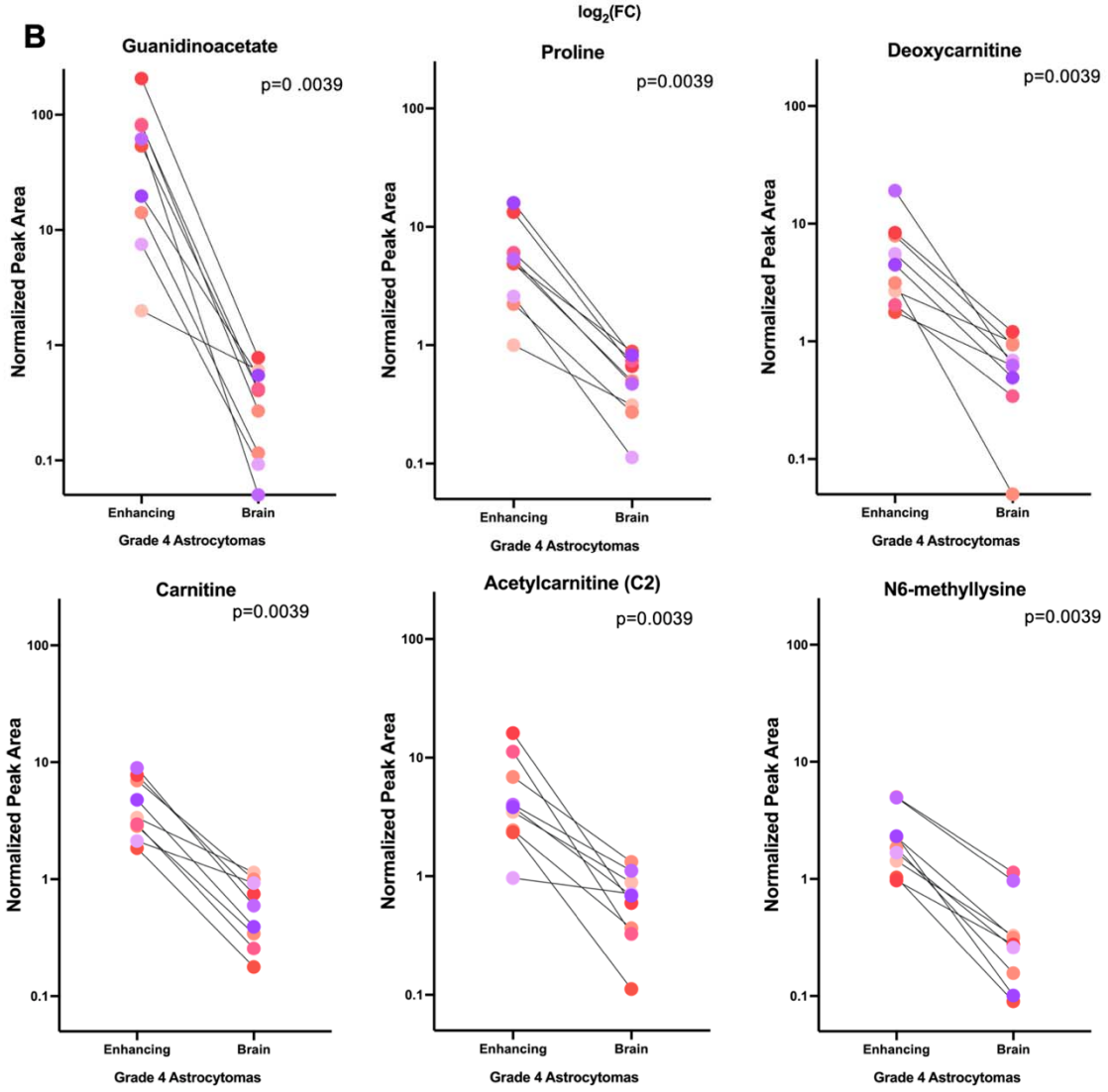
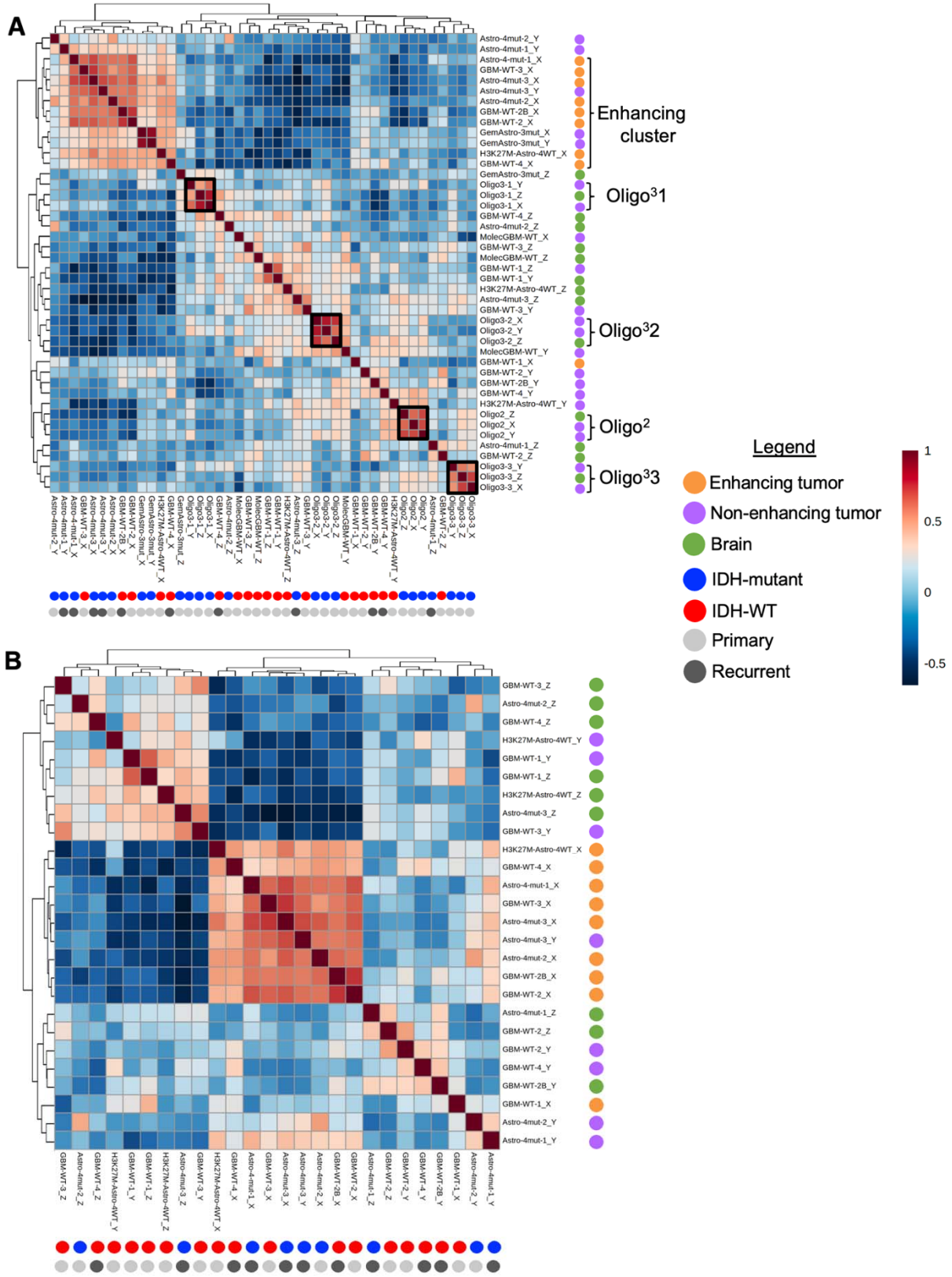
Figure 5. Microdialysate samples correlate based on patient identity and catheter location.